Chain Mobility and Cation Coordination in the Polymer Electrolytes $M[N(CF_3SO_2)_2]_2PEO_n$ with M = Mg, Ca, Sr, and Ba

Åsa Lauenstein and Jörgen Tegenfeldt*

The Ångström Laboratory, Inorganic Chemistry, Uppsala University, Box 538, SE−751 21 Uppsala, Sweden

Received: January 23, 1998; In Final Form: June 30, 1998

The poly(ethylene oxide)-based solid electrolytes $M[N(CF_3SO_2)_2]_2PEO_n$ with M = Mg, Ca, Sr, and Ba and $n = 6-24$ have been examined with proton NMR spectroscopy, DSC, and X-ray diffraction to explore some of their dynamic and structural properties. Changes in salt concentration appear to be more important than changes in ionic radius for properties such as activation energies and correlation times for conformational transformations. Above the glass transition temperature, the fully amorphous samples with M = Mg and $n \leqslant 12$ produce proton NMR spectra that can be decomposed into two components of different width. This is a consequence of the different dynamic properties of cation-coordinated and noncoordinated polymer chain segments. The relationship between the areas of these components results in a maximum effective coordination number for the Mg^{2+} ion between 6 and 7, depending on salt concentration. Some of the initially amorphous samples undergo slow crystallization, producing aged samples with crystalline PEO−salt complexes.

Introduction

Many polymers, such as poly(ethylene oxide), PEO, can dissolve a wide variety of ionic salts to form solid polymer electrolytes. The significant ionic conductivity in the amorphous regions of many of these systems makes them important as electrolyte materials in secondary batteries. Most work in the area has dealt with monovalent cations, in particular lithium ions. Multivalent cations might offer new technological applications, but they also provide added possibilities to study fundamental properties responsible for ionic conduction in polymer electrolytes.

Bakker et al. have studied polymer electrolytes based on high-molecular-weight PEO and salts of divalent cations (Mg^{2+}, Ca^{2+}, Sr^{2+}, and Ba^{2+}) with the bis(trifluoromethane sulfone) imide anion, $N(CF_3SO_2)_2^-$,[1] using DSC, impedance spectroscopy, and infrared spectroscopy to characterize $M[N(CF_3SO_2)_2]_2PEO_9$. The imide ion is flexible and acts as a plasticizer in PEO electrolytes by reducing the tendency for crystallization. It is also chemically and thermally stable and less apt to form ion pairs than the triflate ion, $CF_3SO_3^-$.[2] The alkaline earth cations Mg^{2+}, Ca^{2+}, Sr^{2+}, and Ba^{2+} all have the same charge but differ in ionic radii from 0.66 to 1.34 Å. It was shown in ref 1 that the small radius of the Mg^{2+} ion, comparable to that of the Li^+ ion but with a higher charge, results in striking differences between the larger cation systems and $Mg[N(CF_3SO_2)_2]_2PEO_9$. Bakker et al. proposed a different coordination behavior for the Mg^{2+} ion compared to the larger cations, explained in terms of cation radii and bonding strength, suggesting that PEO is wrapped around the Mg^{2+} ions creating microscopic regions of coordinated and noncoordinated chain segments.[1]

In the present work, we have used proton NMR spectroscopy and spin−lattice relaxation measurements in the rotating frame together with DSC and X-ray diffraction to characterize structural and dynamic properties of the $M[N(CF_3SO_2)_2]_2PEO_n$ system with M = Mg, Ca, Sr, and Ba and $n = 6-24$, where n denotes the oxygen-to-metal ratio. From spin relaxation data we have calculated correlation times, τ_c, and activation energies, E_a, for dynamic processes, such as chain motion and ion−polymer interactions. In a previous study on $La(CF_3SO_3)_3PEO_n$, we have shown how an effective ether oxygen−metal ion coordination number can be estimated on the basis of NMR line-shape analysis.[3] This technique appears to be suitable for testing the coordination behavior proposed in ref 1, and we have, therefore, paid special attention to the magnesium system, $Mg[N(CF_3SO_2)_2]_2PEO_n$.

Experimental Section

Preparation of the PEO Electrolyte Films. Polymer electrolyte $M[N(CF_3SO_2)_2]_2$ PEO_n films were prepared by the mutual solvent method, dried, and handled as described in ref 3. PEO was used as obtained ($M_w = 4 \times 10^6$, BDH polyox 301). The imide salts were prepared from the metal carbonate, and a $HN(CF_3SO_2)_2$ solution was obtained from an aqueous solution of $LiN(CF_3SO_2)_2$, as described in ref 1. Two series of films were prepared: $M[N(CF_3SO_2)_2]_2PEO_9$ with M = Mg, Ca, Sr, and Ba and $Mg[N(CF_3SO_2)_2]_2PEO_n$ with $n = 6$, 9, 12, 16, and 24. From DSC data we know that all newly prepared samples were totally amorphous except for $Mg[N(CF_3SO_2)_2]_2PEO_{24}$.[1] This is in contrast to the corresponding polymer electrolytes with the triflate anion; these are highly crystalline at room temperature.[4] The films used in the measurements reported here were normally 100−200 μm thick.

NMR Spectroscopy. All NMR measurements were performed using a Bruker MSL spectrometer equipped with a 7 T magnet. Proton spectra were recorded at 300 MHz at temperatures between −10 and 130 °C. The rotating-frame spin−lattice relaxation time, $T_{1\rho}$, for the protons was measured with the multiple-pulse method of Rhim, Burum, and Elleman.[5] The Larmor frequency corresponding to the effective spin-locking field was $\nu_1 = 18.5$ kHz. We also studied the $T_{1\rho}$ relaxation by a standard spin-lock experiment, i.e., a 90° pulse immediately followed by a phase-shifted spin-locking pulse of variable length and with $\nu_1 = 62$ kHz. By Fourier transformation of the signal following the locking pulse, we were able to follow the relaxation process separately for the different spectral components.

* Corresponding author. E-mail tegen@kemi.uu.se.

S1089-5647(98)00851-7 CCC: $15.00 © 1998 American Chemical Society
Published on Web 08/12/1998

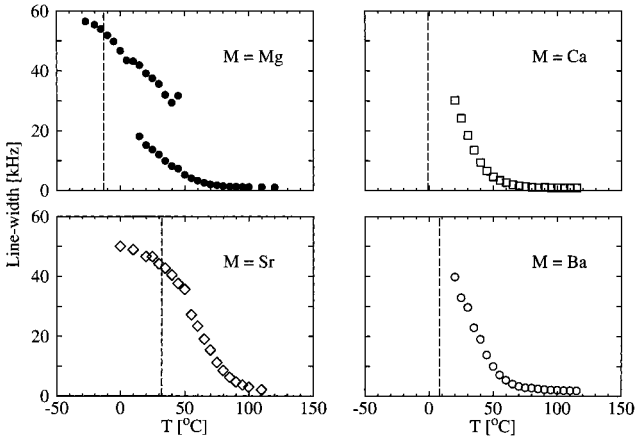

Figure 1. Full line width at half peak height for $M[N(CF_3SO_2)_2]_2PEO_9$ ^1H NMR spectra as a function of temperature. The vertical dashed lines indicate the glass transition temperature for each sample.

DSC Measurements. While kept inside the glovebox, polymer electrolyte film samples of approximately 10 mg were sealed in aluminum pans for DSC analysis. The measurements were made with a Mettler DSC oven, connected to a Mettler TA4000 controller. A flow of nitrogen was maintained over the perforated pan to keep away atmospheric moisture and to remove any decomposition products. The samples were analyzed between −100 and 200 °C with a heating rate of 10 °C/min.

X-ray Diffraction. Both the Mg-containing films and the Mg imide salt were examined by X-ray diffraction on a STOE & CIE GmbH STADI diffractometer with a position-sensitive detector (PSD). The time of exposure to Cu $K\alpha_1$ radiation was 45 to 180 min for a 2θ range of 5−45°. The hygroscopic samples were placed in the sample holder protected by thin Mylar films preventing water absorption from the surrounding air. During measurement, the sample was rotated about the normal to the plane of the sample holder.

Results

Proton NMR Spectra. Each proton NMR spectrum for $M[N(CF_3SO_2)_2]_2PEO_9$ was fitted to a Lorentzian peak (with one exception, see below), and the resulting line widths (full width at half-height) are shown in Figure 1 as a function of temperature. The glass transition temperature, T_g, in the figure for M = Mg, Ca, and Ba, is taken from ref 1. A fresh sample of $Sr[N(CF_3SO_2)_2]_2PEO_9$ turned out to have a higher T_g than that reported in ref 1, according to DSC measurements performed 1 day after preparation, and the dashed line in Figure 1 for M = Sr corresponds to our own measurement. The line width at room temperature is 40 kHz for M = Ba, 47 kHz for M = Sr, and 31 kHz for M = Ca. When the temperature increases, all these spectra show a line narrowing which is most drastic just above T_g, from more than 30 kHz to less than 5 kHz. Both the similarity in the behavior of the samples with M = Ca, Ba, and Sr and the distinctly different behavior of the Mg complex are emphasized in Figure 2 where the line width is shown as a function of $T - T_g$.

The proton spectrum of $Mg[N(CF_3SO_2)_2]_2PEO_9$, in contrast to the samples with larger cations, has two superposed components above about 15 °C, i.e., slightly above T_g. The components have been fitted to peaks of different width: a broad, Gaussian peak and a narrow, Lorentzian peak (Figure 3, fresh). Both components coexist above 15 °C over the entire temperature range studied, but the relative area changes with temperature. When the narrow peak first appears at 15 °C, the broad component accounts for 70% of the total area, while already at 40 °C, the contribution is less than 25%. Above 50 °C, a satisfactory fit to two peaks is no longer possible, although a broad component, approximately 50 kHz wide, is still visible. The proton spectrum immediately after a standard spin-locking experiment on $Mg[N(CF_3SO_2)_2]_2PEO_9$ at 40 °C shows that the two components decay at different rates: for long spin-locking times, only the broad component is detectable (Figure 4). Such a two-component behavior is not seen for any of the samples containing the larger cations.

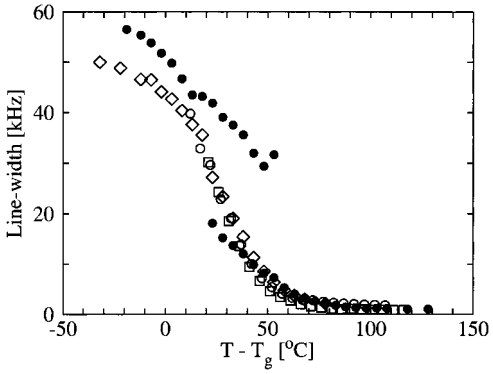

Figure 2. Full line width at half peak height for $M[N(CF_3SO_2)_2]_2PEO_9$ ^1H NMR spectra as a function of $T - T_g$ with M = Mg (●), Ca (□), Sr (◇), and Ba (○).

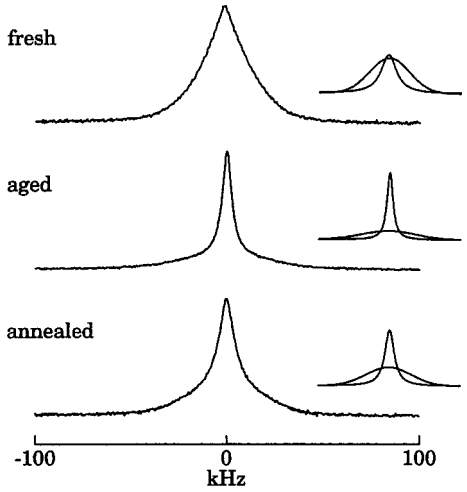

Figure 3. ^1H NMR spectrum of fresh, aged (for 17 months), and annealed (at 135 °C for 6 h) $Mg[N(CF_3SO_2)_2]_2PEO_9$ at room temperature. Each spectrum is shown together with two fitted peaks corresponding to the two components with different polymer chain mobility.

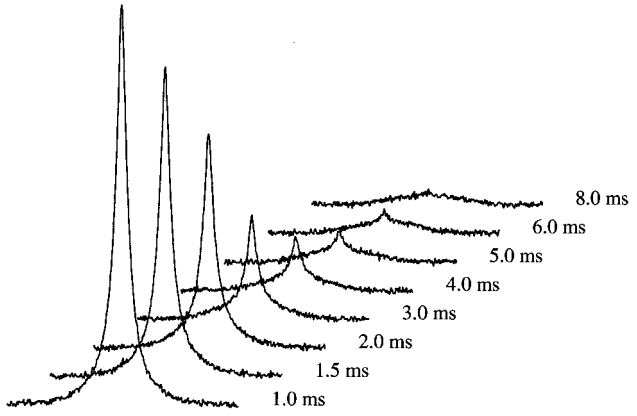

Figure 4. ^1H NMR spectra of fresh $Mg[N(CF_3SO_2)_2]_2PEO_9$ at 40 °C after different times of spin locking.

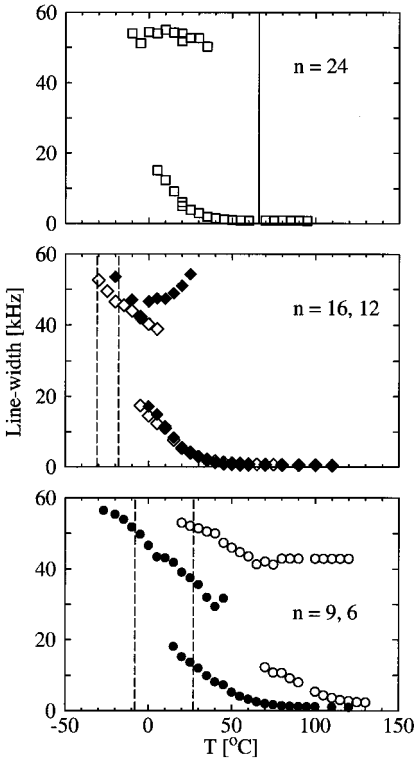

Figure 5. Full line width at half peak height for $Mg[N(CF_3SO_2)_2]_2$-PEO_n ^1H NMR spectra as a function of temperature with $n = 24$ (□), 16 (◆), 12 (◇), 9 (●), and 6 (○). Vertical dashed lines indicate the glass transition temperature for each sample and the vertical solid line the melting temperature of crystalline PEO.

The width and relative area of the components in the spectrum of $Mg[N(CF_3SO_2)_2]_2PEO_9$ also change with time. After 2 months of storage under argon atmosphere, the room-temperature width of the Lorentzian peak has dropped from the initial value of 15 kHz to only 6 kHz, while the Gaussian peak has become slightly broader, the width going up from 39 to 46 kHz. After this storage period, the relative contribution of the broad peak changes very little, from 63% to 60% of the total area. Figure 3 (aged) shows the proton spectrum of the sample after 17 months of storage. The peaks are now 6 and 53 kHz wide, respectively, and the broad peak accounts for only 44% of the total peak area. After annealing a fresh sample at 130 °C for 6 h, the room-temperature spectrum changes in the same direction as during long-time aging: the width of the narrow peak decreases to 9 kHz, and that of the broad peak increases to 45 kHz. The contribution of the broad peak decreases to 53%.

A second series of proton spectra were recorded for $Mg[N(CF_3SO_2)_2]_2PEO_n$ with $n = 6$, 9, 12, and 16, all of which produce totally amorphous samples, and $n = 24$, which contains crystalline PEO in addition to an amorphous complex.[1] The line widths of the spectra are displayed in Figure 5. Again, the signal can be decomposed into a broad and a narrow peak close to T_g. For $n = 6$, the contribution of the broad peak decreases from 80% at 70 °C to less than 40% above 120 °C, while its width is fairly constant. When $n = 12$, two peaks can be fitted to the spectra only between −5 and 5 °C, the relative area of the broad peak decreasing from 60% to 30%. For $n = 16$ the broad peak accounts for 60% at 0 °C and only 20% at 25 °C. For $n = 24$, finally, there are two peaks above 0 °C, where the broad peak of about 50 kHz accounts for 80% of the total area. At room temperature, the contribution is 40%. Above 40 °C, the broad peak decreases rapidly with increasing temperature in both area and width, and above 66 °C, the melting point T_m of pure crystalline PEO, it is no longer visible.

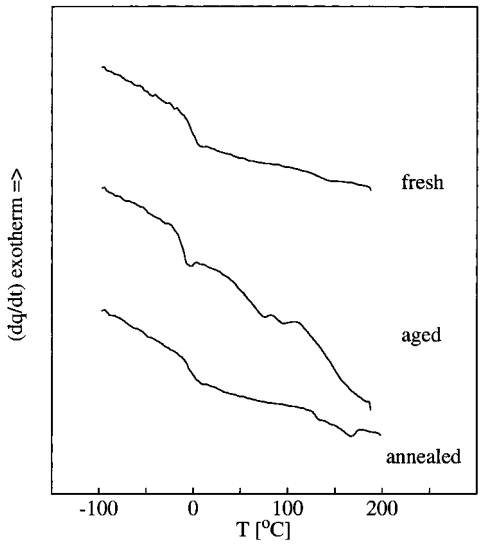

Figure 6. First DSC scan of fresh, aged (for 17 months), and annealed (at 135 °C for 6 h) $Mg[N(CF_3SO_2)_2]_2PEO_9$.

DSC Measurements. The two-component proton NMR spectra from $Mg[N(CF_3SO_2)_2]_2PEO_9$ aroused our curiosity. This type of behavior is well-known for semicrystalline polymers, but $Mg[N(CF_3SO_2)_2]_2PEO_9$ has been reported to be totally amorphous.[1] We, therefore, studied fresh, aged, and annealed samples of $Mg[N(CF_3SO_2)_2]_2PEO_9$ with DSC (Figure 6). The only apparent feature in the DSC trace of the fresh sample is a glass transition at −3 °C, in agreement with ref 1. The second scan of this sample is identical with the first one. The aged sample shows a slightly lower T_g, −13 °C, and additional features are present: two small endotherms at 70 and 90 °C and a large, broad exotherm above 100 °C. The third trace in Figure 4, from the annealed sample, shows a glass transition at −4 °C and again two small exotherms, shifted upward to 130 and 170 °C. For the aged and for the annealed samples, the second DSC scan is close to that from the fresh sample.

DSC measurements were also performed on a $Mg[N(CF_3SO_2)_2]_2PEO_{16}$ sample that had been stored in a glovebox for almost 2 years. The first scan showed a glass transition at −19 °C together with a broad melting endotherm with an onset temperature of 26 °C. The second scan showed neither crystallization nor melting, and the glass transition appeared at −29 °C. The latter value, corresponding to a totally amorphous sample, agrees with ref 1.

Finally, aged samples of $Sr[N(CF_3SO_2)_2]_2PEO_9$ were investigated. DSC traces from a fresh sample showed a completely amorphous sample with $T_g = 32$ °C. When a sample was analyzed 9 days after preparation, however, the glass transition was shifted to a lower temperature, close to 0 °C, as in ref 1. The first scan of this sample showed a sharp melting endotherm with an onset temperature of 100 °C; no crystallization or melting was observed in the second scan. Similar features were found after almost 2 years of storage: a T_g close to 0 °C, but a broader melting already at 80 °C. Again, no crystallization or melting occurred during the second DSC scan. The NMR experiments reported here for this material were all performed on a fresh, totally amorphous sample.

X-ray Diffraction. X-ray diffraction was performed on the $Mg[N(CF_3SO_2)_2]_2PEO_9$ fresh, aged, and annealed samples (Figure 7). The fresh sample gives a broad amorphous profile with maxima at 2θ equal to 14° and 21°, and no sharp Bragg reflections are observed. In contrast, the aged as well as the annealed samples give sharp Bragg peaks distributed within the

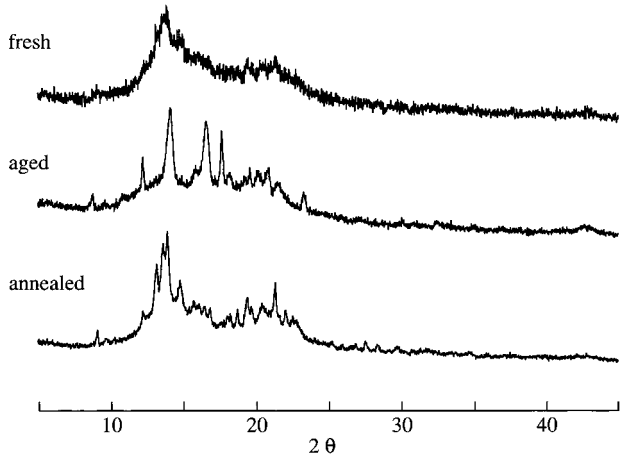

Figure 7. X-ray diffraction pattern of fresh, aged (for 17 months), and annealed (at 135 °C for 6 h) $Mg[N(CF_3SO_2)_2]_2PEO_9$ at room temperature.

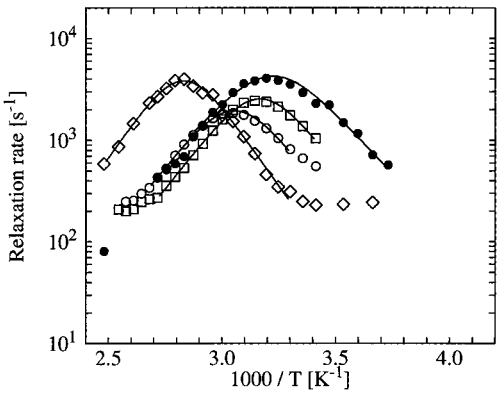

Figure 8. ^{1}H relaxation rate in the rotating frame as a function of inverse temperature for $M[N(CF_3SO_2)_2]_2PEO_9$ with M = Mg (●), Ca (□), Sr (◇), and Ba (○).

2θ range covered by the amorphous profile from the fresh sample. The relative intensities of the peaks, though, are quite different in the aged and the annealed sample. These peaks are not from precipitated salt, since a diffractogram from polycrystalline magnesium imide salt gave Bragg reflections between 10° and 40° with no clear resemblance to the polymer electrolyte samples. In addition, it is clear that the peaks in Figure 7 cannot be attributed to crystalline PEO, which has characteristic peaks at about 20° and 25°.[6]

***T*$_{1\rho}$ Relaxation Measurements.** The temperature dependence of the proton rotating-frame spin−lattice relaxation rate, $1/T_{1\rho}$, is shown in Figure 8 for $M[N(CF_3SO_2)_2]_2PEO_9$ as a function of cation and in Figure 9 for $Mg[N(CF_3SO_2)_2]_2PEO_n$ as a function of concentration. Although the line shape of the proton NMR spectra for the totally amorphous samples with M = Mg and $n \leqslant 16$ reveals the coexistence of two local regions with different dynamic properties, the $T_{1\rho}$ measurements provided reliable data only for the slowly relaxing component. Therefore, for these samples, only the slowly relaxing component is included in Figures 8 and 9.

The semicrystalline sample with $n = 24$ (Figure 9a) shows a biexponential decay of the spin-locked magnetization below T_m of crystalline PEO. Standard spin-lock experiments at different temperatures, similar to those in Figure 4 for $n = 9$, allowed an unambiguous assignment of the two components to the broad and the narrow component of the NMR spectrum, respectively. The broad component reaches a relaxation rate maximum at a higher temperature, 45 °C, than the narrow, 20 °C.

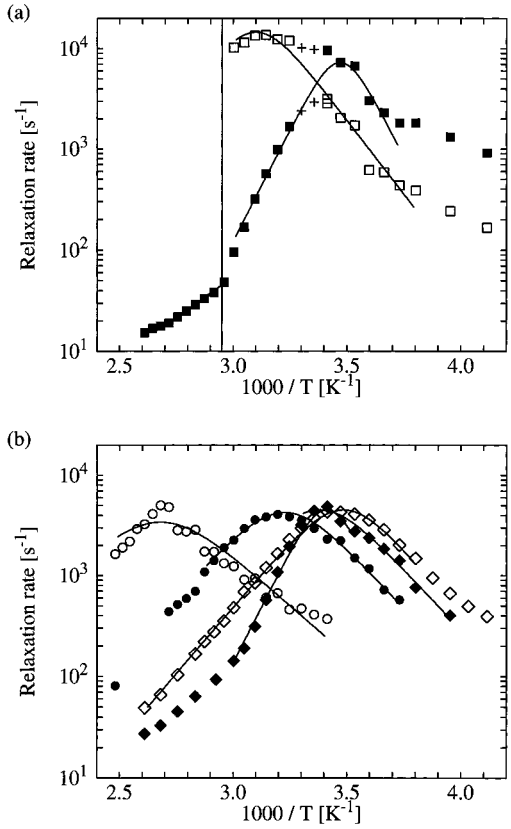

Figure 9. ^{1}H relaxation rate in the rotating frame as a function of inverse temperature for $Mg[N(CF_3SO_2)_2]_2PEO_n$ with (a) $n = 24$, broad (□), and 24, narrow (■), and (b) $n = 16$ (◆), 12 (◇), 9 (●), and 6 (○). The vertical solid line indicates the melting temperature of crystalline PEO.

The source of the proton relaxation in the polymer electrolytes is a random fluctuation of the proton−proton dipole−dipole interaction caused predominantly by the polymer-chain motion, and a $1/T_{1\rho}$ maximum corresponds to a fluctuation rate on the order of the Larmor frequency ν_1 in the effective spin-locking field. The temperature for the $1/T_{1\rho}$ maximum, T_{max}, for M = Mg, Ca, and Ba increases from 40 to 55 °C when the ionic radius increases. M = Sr shows a T_{max} of 70 °C. We assume the correlation time, τ_c, of the polymer chain motion to be related to $1/T_{1\rho}$ via an equation of the form[7]

$$\frac{1}{T_{1\rho}} = \Delta M_2 \left\{ \frac{\tau_c}{1+4\omega_1^2\tau_c^2} + \frac{5}{3}\frac{\tau_c}{1+\omega_0^2\tau_c^2} + \frac{2}{3}\frac{\tau_c}{1+4\omega_0^2\tau_c^2} \right\} \quad (1)$$

where $\omega_1 = 2\pi\nu_1$ and ω_0 are the angular Larmor frequencies of the protons, in the effective spin-locking field and the static magnetic field, respectively, and ΔM_2 is the difference between the limiting values of the second moment of the NMR spectrum at low and high temperatures. The τ_c values for $M[N(CF_3SO_2)_2]_2PEO_9$ derived using eq 1 are shown as a function of cation and inverse temperature in Figure 10. The rate of motion, $1/\tau_c$, at a given temperature does not differ much for M = Mg, Ca, and Ba, although it decreases with increasing ionic radius. For M = Sr, the $1/\tau_c$ is somewhat lower than for the other ions.

An activation energy E_a for the chain motion can be determined by fitting eq 1 together with an Arrhenius expression for τ_c

$$\tau_c = \tau_0 \exp(E_a/RT) \quad (2)$$

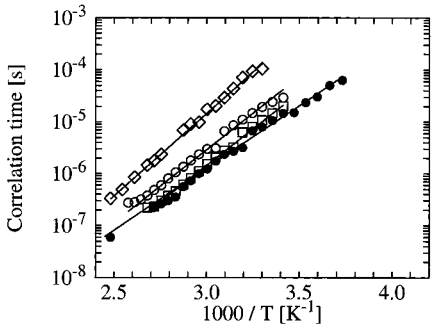

Figure 10. Correlation times derived from $1/T_{1\rho}$ as a function of inverse temperature for $M[N(CF_3SO_2)_2]_2PEO_9$ with M = Mg (●), Ca (□), Sr (◇), and Ba (○).

TABLE 1: Activation Energy and Related Parameters for $M[N(CF_3SO_2)_2]_2PEO_9$ from $T_{1\rho}$ Relaxation Data for Protons

M	E_a (kJ/mol)	T_{max} (°C)	τ_0 (s)	ΔM_2 (s^{-2})
Mg	46	40	8×10^{-14}	2.0×10^9
Ca	54	45	5×10^{-15}	1.2×10^9
Sr	61	70	4×10^{-15}	1.8×10^9
Ba	54	55	1×10^{-14}	9.1×10^8

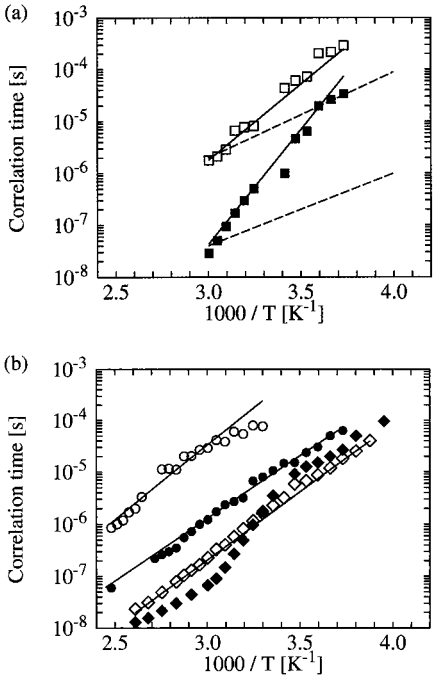

Figure 11. Correlation times derived from $1/T_{1\rho}$ as a function of inverse temperature for $Mg[N(CF_3SO_2)_2]_2PEO_n$ with (a) $n = 24$, broad (□), and 24, narrow (■), and (b) $n = 16$ (◆), 12 (◇), 9 (●), and 6 (○). The two dashed lines in (a) indicate correlation times derived from NMR data for crystalline (top trace) and amorphous PEO (bottom trace) in ref 9.

to the experimental spin relaxation data. The fits for the $M[N(CF_3SO_2)_2]_2PEO_9$ system are indicated in Figure 10 as solid lines, and the resulting parameters are displayed in Table 1 together with T_{max}. E_a increases with ionic radius from 46 kJ/mol for M = Mg to 54 kJ/mol for M = Ba, except that M = Sr shows a still higher activation energy of 61 kJ/mol.

Corresponding data for $Mg[N(CF_3SO_2)_2]_2PEO_n$ with $n = 6-24$ are presented in Figure 11 and Table 2. At least for the most concentrated samples τ_c is concentration-dependent: the rate of motion is about 100 times higher for $n = 12$ than for $n = 6$. The samples with $n = 12$ and $n = 16$ and the amorphous component in $n = 24$, however, are very close, corresponding to the close resemblance of the $T_{1\rho}$ data in Figure 9. The

TABLE 2: Activation Energy and Related Parameters for $Mg[N(CF_3SO_2)_2]_2PEO_n$ from $T_{1\rho}$ Relaxation Data for Protons

n	E_a (kJ/mol)	T_{max} (°C)	τ_0 (s)	ΔM_2 (s^{-2})
6	55	100	8×10^{-14}	2.0×10^9
9	46	40	8×10^{-14}	2.0×10^9
12	50	20	3×10^{-15}	2.1×10^9
16 ($< T_{max}$)	46	20	3×10^{-14}	2.1×10^9
16 ($> T_{max}$)	85		3×10^{-21}	2.1×10^9
24 (am, $< T_m$)	85	20	2×10^{-21}	3.4×10^9
24 (am, $> T_m$)	30			
24 (cryst)	56	45	3×10^{-15}	6.7×10^9

crystalline component from $n = 24$ has a longer τ_c than the amorphous component. Figure 11a includes data for crystalline and amorphous PEO (dashed lines).[9] Close to T_m of PEO, τ_c for crystalline and amorphous material in $Mg[N(CF_3SO_2)_2]_2PEO_{24}$ almost coincides with the data for PEO. Here, the τ_c ratio between crystalline and amorphous material is 100. At lower temperatures, the data differ significantly, and the ratio between τ_c in crystalline and amorphous $Mg[N(CF_3SO_2)_2]_2PEO_{24}$ has decreased to 10 at about 20 °C.

The E_a values in $Mg[N(CF_3SO_2)_2]_2PEO_n$ are about 50 kJ/mol for $n \leq 12$. T_{max} decreases from 100 °C for $n = 6$ to 20 °C for $n = 12$ and 16. For $n = 16$, the relaxation rate dependence on $1/T$ is asymmetric with different slopes and hence different E_a below and above T_{max}, 46 and 85 kJ/mol. When $n = 24$, the crystalline material has a T_{max} of 45 °C and an E_a of 56 kJ/mol, while the amorphous phase has a T_{max} of 20 °C. E_a in the amorphous phase is 85 kJ/mol below T_m of PEO, but only 30 kJ/mol above this temperature.

Discussion and Conclusions

Ionic Radius Effects. The proton NMR spectra for $M[N(CF_3SO_2)_2]_2PEO_n$ exhibit a drastic line narrowing close to T_g (Figures 1 and 2), discussed earlier for similar systems,[3,10] where the line narrowing at T_g is attributed to the onset of local segmental motion in the polymer chain. The line width as a function of $T - T_g$ for $n = 9$ (Figure 2) demonstrates a striking similarity between M = Ca, Sr, and Ba. This is clear evidence that the line narrowing really is associated with the polymer dynamics occurring above T_g. The line width behavior of the sample with M = Mg deviates from that of the other three, but the major part of the line narrowing still occurs in the vicinity of that of the other samples.

As expected, M = Ca, Sr, and Ba have room-temperature NMR line widths that are far larger than the 5 kHz for pure amorphous PEO, since the segmental mobility of the polymer chains is reduced due to interactions between the cations and the ether oxygens in the polymer backbone.[11] Since cation−anion interactions will reduce the capability of the cations to coordinate these oxygens, the extent of the line broadening depends on both cation−anion and cation−polymer interactions. For the polymer electrolytes in the present paper the line broadening at a given temperature increases with increasing cation radius (Figure 1). The largest cations, Ba^{2+} and Sr^{2+} (ionic radii 1.34 and 1.12 Å, respectively), are able to coordinate a large number of polymer ether oxygens, efficiently restricting the segmental mobility of the polymer chain. The Ca^{2+} ion (ionic radius 0.99 Å) will be less efficient, since it cannot coordinate as much of the polymer chain as the larger ions.

Still, this trend does not explain the two-component nature of the proton NMR spectrum for M = Mg. The existence of two components above T_g, corresponding to PEO chain segments with different relaxation properties, is confirmed by the spin-locking data at 40 °C in Figure 4. This behavior has

frequently been observed in polymers and is often explained by the presence of both crystalline and amorphous phases with different chain mobility. In fact, a proton spectrum of $Mg[N(CF_3SO_2)_2]_2PEO_9$ at room temperature resembles that of PEO, also consisting of two superposed peaks, one broad and one narrow. Pure PEO, however, has macroscopic regions of amorphous and crystalline polymer with different dynamic properties, and the broad peak from crystalline material disappears on heating above T_m of pure PEO, 66 °C.[9] However, in $Mg[N(CF_3SO_2)_2]_2PEO_9$ the broad component is visible up to at least 120 °C. The first DSC trace in Figure 6 and the first X-ray diffractogram in Figure 7 prove that the sample is completely amorphous, although the diffractogram shows diffuse peaks indicating at least some degree of order. This would also be expected from a comparison with the phase diagram of $Li[N(CF_3SO_2)_2]_2PEO_n$, which exhibits a crystallinity gap for $8 \leqslant n \leqslant 10$; these samples had, additionally, been stored in room-temperature several months prior to measurement to allow crystallization.[12] We therefore suggest that the two components correspond to coordinated and noncoordinated chain segments of the amorphous polymer, where the coordinated segments exhibit a restricted mobility with the polymer chain tightly wrapped around the Mg^{2+} ion. In a previous study, two such regions could be resolved in an NMR experiment in $La(CF_3SO_3)_3PEO_n$.[3] This is because the upper limit for the cationic diffusion derived from the ionic conductivity provided a minimum residence time between successive cation jumps 2 orders of magnitude longer than the inverse of the relevant line widths in the NMR experiment. Since both the ionic conductivity and the proton NMR line width are comparable in the $La(CF_3SO_3)_3PEO_n$ and $Mg[N(CF_3SO_2)_2]_2PEO_n$ systems, we propose that the same approach can be used here. The consequences for determination of coordination numbers of the Mg^{2+} ion will be discussed below.

The effect of ionic radius on the macroscopic properties of $M[N(CF_3SO_2)_2]_2PEO_n$ has been demonstrated by Bakker et al.[1] DSC data show that all samples with $n = 9$ are completely amorphous. The large Ba^{2+} ions are able to coordinate simultaneously most of the ether oxygens of the polymer chain. The chains are, therefore, quite inflexible, and this results in a rigid sample with a high T_g. On the other hand, in $Mg[N(CF_3SO_2)_2]_2PEO_9$ a smaller fraction of the ether oxygens will be coordinated by Mg^{2+} than by Ba^{2+} in the previous case. This results in large sections of the polymer chain being noncoordinated and, therefore, rather flexible. Thus, $Mg[N(CF_3SO_2)_2]_2PEO_9$ has the lowest T_g of the electrolytes studied, despite the strong interactions expected between the polymer ether oxygens and the very small Mg^{2+} ion. The conductivity in $M[N(CF_3SO_2)_2]_2PEO_9$ follows the same trend as T_g, and e.g. for M = Mg, the conductivity is considerably higher than for M = Ba.[1] Again, the presence of flexible chain segments for M = Mg appears to overcome in part the effect of the strong interaction between Mg^{2+} and the ether oxygens, and as a result, a high conductivity is obtained. At lower salt concentrations such as $M[N(CF_3SO_2)_2]_2PEO_{40}$, the situation is reversed because of the presence of noncoordinated polymer sections in all samples. At this concentration, Mg^{2+} shows the lowest conductivity due to the strong interactions between the cation and the polymer chain, while the large radius of Ba^{2+} results in weaker ion−polymer interactions and a high conductivity.[1]

In ref 1, ionic conductivity and T_g in $M[N(CF_3SO_2)_2]_2PEO_9$ show a clear dependence on the cation radius: a larger radius resulted in lower conductivity and higher T_g. Nevertheless, in our NMR data, the expected related trends for line shape and relaxation parameters appear to be valid only for M = Mg, Ca, and Ba. Apart from the substantially higher T_g than expected,[1] $Sr[N(CF_3SO_2)_2]_2PEO_9$ has a considerably broader proton spectrum than M = Ba at a given temperature. Additionally, in the NMR relaxation data, M = Sr shows the highest values of E_a, T_{max}, and τ_c. The DSC data may provide a clue to this discrepancy. Newly prepared $Sr[N(CF_3SO_2)_2]_2PEO_9$ is completely amorphous, but after only 9 days, crystalline material has formed in the sample. The process is thus considerably faster than for M = Mg, where crystallinity due to aging was first noted after 2 months; NMR spectra of samples with M = Ca and Ba, furthermore, showed no changes even after 1 year of storage. We suggest that the fresh M = Sr samples are very far from equilibrium and may show properties quite different from those expected from considering the ionic radius only.

The relaxation rate maxima in Table 1 shift to higher temperatures with increasing ionic radius. With the exception of M = Sr, this effect is not very large. The parameter E_a reflects the activation energy for the polymer chain movements causing spin relaxation. Amorphous PEO has $E_a = 28$ kJ/mol, reflecting the flexibility of the noncoordinated chain segments.[9] The introduction of salt in $M[N(CF_3SO_2)_2]_2PEO_9$ results in a higher E_a for the coordinated PEO chains. This effect is less pronounced for M = Mg but more evident for the larger cations; the highest E_a is found for M = Sr with 61 kJ/mol. The τ_c values are 10−1000 times longer for the PEO−salt complexes than for pure amorphous PEO over the temperature range of our measurements. The values for $M[N(CF_3SO_2)_2]_2PEO_9$ are, in fact, quite close to those for crystalline PEO,[9] indicating a restriction of the polymer chain mobility in the complex comparable to that caused by the formation of crystalline material. Once a certain amount of salt has been introduced into the system, the effect of ionic radius on τ_c is quite small; the exception is, again, M = Sr.

Concentration Effects. In $Mg[N(CF_3SO_2)_2]_2PEO_n$ T_g increases with salt content.[1] This is reflected in the NMR data in Figure 5: an increased salt concentration results in broader lines for $n \leqslant 12$. The broad component in $n = 24$ is not visible above T_m of pure PEO, and therefore we assign it to the crystalline PEO present.[1] Crystalline PEO has a proton spectral component of about the same line width, and the relaxation data for this component have a T_{max} of 39 °C,[9] close to that found here, 45 °C. Yet E_a for crystalline PEO is considerably larger in $Mg[N(CF_3SO_2)_2]_2PEO_{24}$, 56 kJ/mol, than in ref 9, 32 kJ/mol. Close to T_m, τ_c for the crystalline phase is comparable in the two different samples, but at 0 °C, the rate of motion is about an order of magnitude slower for crystalline material in $Mg[N(CF_3SO_2)_2]_2PEO_{24}$.

Semicrystalline $Mg[N(CF_3SO_2)_2]_2PEO_{24}$ has an E_a of 85 kJ/mol below T_m, while the samples with $n \leqslant 16$ all have E_a in the range of only 46−55 kJ/mol. In the amorphous regions of the $n = 24$ sample, however, the chain mobility is restricted not only by ion−polymer interactions but also by the presence of crystalline material. The same effect has earlier been observed in the $Pb(CF_3SO_3)_2PEO_n$ system.[10] The actual salt concentration in the amorphous regions of the semicrystalline sample will be considerably higher than $n = 24$. Once the crystalline phase has melted, the sample shows a single $T_{1\rho}$ (Figure 9). The actual concentration in the homogeneous melt is overall equal to $n = 24$, and due to the absence of crystalline material and the lower number of interacting ions per ether oxygen, the sample is now less rigid and the relaxation is slower than below T_m. Above T_m of the crystalline phase, E_a decreases to 30 kJ/mol, close to the value of pure PEO.[9] In other words,

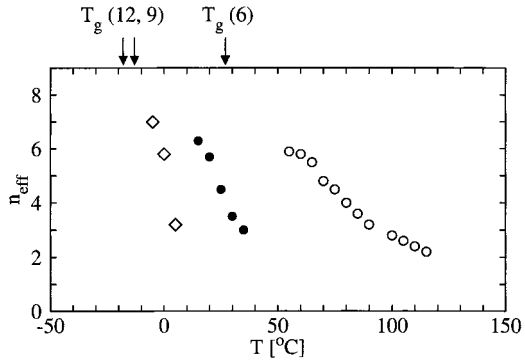

Figure 12. Effective coordination number for $Mg[N(CF_3SO_2)_2]_2PEO_n$ with $n = 12$ (◇), 9 (●), and 6 (○). Glass transition temperatures are indicated in the figure.

decreasing the salt concentration in the $Mg[N(CF_3SO_2)_2]_2PEO_n$ system results in a roughly downward trend for E_a, from 55 kJ/mol for $n = 6$ to 30 kJ/mol for $n = 24$ above T_m.

$Mg[N(CF_3SO_2)_2]_2PEO_n$ with $6 \leqslant n \leqslant 16$ is amorphous,[1] in contrast to $LiN(CF_3SO_2)_2PEO_n$ where a crystalline complex with $n = 6$ exists and where a sample with $n \geqslant 12$ contains crystalline PEO.[12] Since the Mg^{2+} and Li^+ ions are of comparable size, 0.66 and 0.68 Å, we ascribe the greater ability of the Mg^{2+} ion to coordinate amorphous PEO segments to the difference in charge. Above T_g, $Mg[N(CF_3SO_2)_2]_2PEO_n$ with $n = 6$ and 12 gives spectra with the same two-component behavior as $n = 9$, and consequently, we assign the two components to coordinated and noncoordinated PEO. For $n = 16$, two components are again present, but here $T_{1\rho}$ data result in different E_a above and below T_{max} . We made no further investigations of the morphology for $n = 16$ and draw no conclusions about the kinetics of the formation of crystalline material. Nevertheless, these considerations prevent us from assigning the two NMR components from $n = 16$ in the same straightforward manner as for $n \leqslant 12$.

Coordination Numbers. From the relative area of the two proton NMR spectral components in $Mg[N(CF_3SO_2)_2]_2PEO_n$ with $n = 6$, 9, and 12, we have calculated an average coordination number (Figure 12). At 5 °C, the most dilute sample with $n = 12$ shows an effective coordination number, n_{eff}, of 7.0; n_{eff} is defined as the fraction of polymer chain segments coordinated to, or closely interacting with, the Mg^{2+} ion. The maximum n_{eff} for $n = 9$ at 15 °C is 6.3. In the $n = 6$ sample, finally, each Mg^{2+} ion coordinates as a maximum 5.9 ether oxygens at 55 °C or almost all oxygens present. IR spectroscopy has shown the presence of noncoordinated ether oxygens in $Mg[N(CF_3SO_2)_2]_2PEO_6$ at room temperature,[1] which supports the conclusion that the average coordination number is somewhat less than 6.

For all concentrations n_{eff} is highly temperature dependent: at 115 °C, two components can still be derived from the proton spectrum of $n = 6$, but the number of coordinated segments per Mg^{2+} is now only 2.2. A similar effect has been observed in $La(CF_3SO_3)_3PEO_n$.[3] With increasing temperature, PEO tends to transform from gauche to trans at the O−C−C−O dihedral angle, the polymer chain straightens, and consecutive ether oxygens are located on opposite sides of the chain. This reduces the number of favorable coordination sites[13] and limits the possible coordination number at high temperatures for all salt concentrations.

We conclude that in $Mg[N(CF_3SO_2)_2]_2PEO_6$ at 55 °C almost all ether oxygens coordinate a cation, and we suggest this to be valid also at lower temperatures. Furthermore, IR spectroscopy has detected ion pairs in this sample at room temperature.[1] This implies that the Mg^{2+} ion coordinates five or six ether oxygens and one or more oxygens from one or two anions. In crystal structures of PEO−salt complexes the cation is often in the center of a PEO helix, coordinating a number of consecutive ether oxygens but also one or two anions.[8] In the more dilute samples with $n \geqslant 9$, enough ether oxygens per cation are available to fill all possible coordination sites at the Mg^{2+} ions, excluding anion coordination. For these concentrations no ion pairs are detected.[1] Consequently, these samples initially show a higher fraction of cation-coordinated chain segments than $n = 6$, and the highest effective coordination number is found for $n = 12$.

An overall cation−ether oxygen coordination number of six or seven is supported by the information derived from $T_{1\rho}$ data. When $n = 12$, 50% of the polymer segments are already noncoordinated. A further decrease in salt concentration should therefore only have a minor effect on dynamic properties such as T_{max} and the rate of motion. In fact, both T_{max} and τ_c for $n = 16$ and the amorphous component in $n = 24$ are close to those of $n = 12$. In the more concentrated samples, the fraction of noncoordinated chain segments decreases rapidly, from almost 50% for $n = 12$ to less than 5% for $n = 6$. As a result, the motion slows down strongly with increasing salt concentration: at 50 °C, the τ_c values for $n = 12$ and 6 differ by more than 2 orders of magnitude. Additionally, T_{max} increases from 20 °C for $n = 12$ to 100 °C for $n = 6$. A further support is the T_g values reported in ref 1. Going from $n = 24$ to 12 causes an increase in T_g only from −36 to −23 °C, while for $n = 6$, T_g is as high as 17 °C.

In the present study, we have made no attempts to estimate the effective coordination number for the Ca^{2+}, Sr^{2+}, and Ba^{2+} cations in $M[N(CF_3SO_2)_2]_2PEO_9$. The tendency to form ion pairs with the anion increases with cation radius, even though the smaller cations might be expected to interact more strongly with the anion.[1] As a consequence, the larger ionic radius does not necessarily lead to a higher ether oxygen−cation coordination number than for Mg^{2+}, but coordination sites on the cation can be occupied by oxygens from the anion. Still, for $n \leqslant 9$, only coordinated PEO is found for M = Ca, Sr, and Ba, which implies a ether oxygen−cation coordination number close to 9;[1] the total coordination number, including anion oxygens, must therefore be higher than 9.

Aging Effects. DSC and X-ray diffraction data show that fresh $Mg[N(CF_3SO_2)_2]_2PEO_9$ is totally amorphous: it has neither melting endotherms nor sharp Bragg reflections. For the aged and the heat-treated samples, the DSC traces show that T_g is not much affected by aging. The annealed sample has a T_g close to the fresh sample, indicating that the salt concentration in the amorphous phase is approximately the same in both samples; T_g has previously been found to be concentration dependent.[1] The lower T_g in the aged sample suggests that here the amorphous phase has a somewhat lower salt concentration. At higher temperatures, endotherms are visible in both the aged and the heat-treated sample. Such endotherms in a polymer electrolyte are usually attributed to the melting of crystalline polymer, precipitated salt, or crystalline polymer−salt complexes. Pure PEO, however, melts at 66 °C, and thus this possibility can be ruled out. Formation of crystalline PEO would, furthermore, decrease the oxygen-to-cation ratio in the amorphous phase, causing an increase of T_g in the aged sample; here, T_g is lower than in the fresh sample. Finally, the characteristic peaks from crystalline PEO are not present in Figure 7.[6] T_m of $Mg[N(CF_3SO_2)_2]_2$ is not known to us; but

there was no sign of salt precipitation in the samples, and furthermore there is no agreement between an X-ray pattern of the pure salt and the patterns in Figure 7. The Bragg reflections from the aged and the annealed samples must, therefore, arise from a crystalline PEO−salt complex. Such a complex could also be present in the aged $Mg[N(CF_3SO_2)_2]_2PEO_{16}$ sample, where the melting has an onset temperature considerably lower than T_m of PEO.

We ascribe the components in the proton NMR spectrum from fresh $Mg[N(CF_3SO_2)_2]_2PEO_9$ to polymer segments of different mobility but in the same amorphous phase. Spectra from the aged and annealed samples still show two components, although the line widths and area relations have changed. The width of the narrow peak, attributed to noncoordinated segments, has decreased to less than half its initial value in the aged sample, indicating a substantially increased flexibility of the polymer chain. The broad peak is about 20% wider than in the fresh sample, and its relative area has decreased from 63% to 44%. Apparently, the same number of Mg^{2+} ions interact more strongly with a decreasing number of PEO segments when the sample gets older. At the same time, X-ray diffraction shows that aging leads to a higher degree of order. The effects of annealing and aging are qualitatively the same.

We therefore suggest that aging at room temperature as well as annealing at an elevated temperature induces changes in the $Mg[N(CF_3SO_2)_2]_2PEO_9$ chain configuration, from a disordered amorphous system with only short-range order to a semicrystalline system containing PEO−magnesium salt complexes with an ether oxygen-to-cation ratio close to 9, that of the amorphous material. This conclusion is supported by the fact that T_g changes little in the different samples. The quite different X-ray diffraction patterns from the aged and annealed samples, though, indicate that the resulting configuration is not necessarily the same in the two cases. For $n = 16$, T_g increases when crystalline material is formed, suggesting a increased salt concentration in the amorphous phase. A plausible explanation would be that the crystalline material consists of pure PEO; this does not agree, however, with the melting endotherm found at 26 °C. Together with the many discrepancies in the $T_{1\rho}$ data, this implies that $Mg[N(CF_3SO_2)_2]_2PEO_{16}$ is a complex, multiphase system, possibly containing several crystalline phases of varying compositions.

No crystalline magnesium imide−PEO complexes have, as far as we know, been reported, although there are crystalline $Li[N(CF_3SO_2)_2]_2PEO_n$ compounds with $n = 2$, 3, and 6.[12] It is interesting to note that these complexes of lithium salt with PEO ($M_w = 4000$) were reported for samples that had been heat treated at 130−160 °C and stored at room temperature for several months prior to measurement; i.e., they had undergone the same treatment as our annealed and aged samples. The formation of crystalline material in $Mg[N(CF_3SO_2)_2]_2PEO_9$ is very slow: the earliest effects were visible in proton NMR spectra after 2 months of storage at room temperature. The initial drying temperature of the sample, 105 °C, did not induce any of the above changes, but at 130 °C, the rate of the process was apparently greatly enhanced.

Aging processes were also observed for $Sr[N(CF_3SO_2)_2]_2PEO_9$, although considerably faster than for M = Mg. The newly prepared M = Sr sample shows several deviations from the behavior expected from the trends exhibited by the other ions, suggesting that the sample is far from equilibrium. The endothermic melting visible in DSC indicates that a crystalline phase is formed after only a week of storage. The onset temperature for the melting is considerably higher than that of pure PEO, which rules out the formation of the pure crystalline polymer. In the second DSC scan, the endothermic peak is no longer visible, but it appears again after some time of storage. This indicates that the peak does not arise from the decomposition or melting of salt but that the process is reversible with a slow reformation of the crystalline phase. We thus conclude that the peak arises from the melting of a crystalline $Sr[N(CF_3SO_2)_2]_2PEO_n$ complex, although no such complexes have yet been reported. Because of the lower T_g in the aged sample, we suggest that the crystalline complex has an n lower than 9.

Summary

Proton NMR parameters such as line width, correlation times, and activation energies for dynamic processes in the polymer chain have been studied in the polymer electrolyte system $M[N(CF_3SO_2)_2]_2PEO_n$. The effects of ionic radius and concentration correspond to the changes in T_g and ionic conductivity reported by Bakker et al.[1] The concentration dependence in the $Mg[N(CF_3SO_2)_2]_2PEO_n$ system is most pronounced for high salt concentrations, where correlation times for the polymer chain motion are 2 orders of magnitude larger for $n = 6$ than for $n = 12$.

NMR spectroscopy can distinguish between coordinated and noncoordinated polymer-chain segments in $Mg[N(CF_3SO_2)_2]_2PEO_n$ with $n = 6$, 9, and 12. Close to T_g, the Mg^{2+} ions in the most concentrated sample coordinate almost all ether oxygens, but the coordination number decreases at higher temperatures due to conformational changes of the polymer chain. The highest coordination number found for $n = 12$ is seven, resulting in almost equal fractions of coordinated and noncoordinated chain segments.

Some of the initially amorphous samples with M = Mg and Sr and $n = 9$ and 16 undergo slow crystallization, producing crystalline polymer−salt complexes of unknown compositions. Crystalline complexes have, though, been reported for aged samples in the related $Li[N(CF_3SO_2)_2]_2PEO_n$ system.[12]

Acknowledgment. This work was supported by the Swedish Natural Science Research Council and the Swedish Research Council for Engineering Sciences, which is hereby gratefully acknowledged. Thanks are due to Helena Berg for skillful assistance with the X-ray diffraction measurements and to Dr. Jan Lindgren and Dr. Albert Lauenstein for valuable discussions.

References and Notes

(1) Bakker, A.; Gejji, S.; Lindgren, J.; Hermansson, K.; Probst, M. *Polymer* **1995**, *36*, 4371.

(2) Armand, M.; Gorecki, W.; Andréani, R. In *Proceedings of the 2nd International Symposium on Polymer Electrolytes*; Scrosati, B., Ed.; Elsevier: New York, 1990; p 91.

(3) Lauenstein, Å.; Tegenfeldt, J. *J. Phys. Chem. B* **1997**, *101*, 3311.

(4) Bakker, A.; Lindgren, J.; Hermansson, K. *Polymer* **1996**, *37*, 1871.

(5) Rhim, W. K.; Burum, D. P.; Elleman, D. D. *Phys. Rev. Lett*. **1976**, *37*, 1764.

(6) Wendsjö, Å.; Yang, H. In *Proceedings of the 2nd International Symposium on Polymer Electrolytes*; Scrosati, B., Ed.; Elsevier: New York, 1990; p 225.

(7) Abragam, A. *The Principles of Nuclear Magnetism;* Oxford University Press: London, 1961.

(8) Bruce, P. G. *Faraday Discuss. Chem. Soc.* **1989**, *88*, 91.

(9) Johansson, A.; Tegenfeldt, J. *Macromolecules* **1992**, *25*, 4712.

(10) Johansson, A.; Tegenfeldt, J. *J. Chem. Phys.* **1996**, *104*, 5317.

(11) Johansson, A.; Wendsjö, Å.; Tegenfeldt, J. *Electrochim. Acta* **1992,** *37*, 1487.

(12) Vallée, A.; Besner, S.; Prud'homme, J. *Electrochim. Acta* **1992**, *37*, 1579.

(13) Bernson, A. *Comprehensive Summaries of Uppsala Dissertations from the Faculty of Science and Technology* **1996**, *182*, 14.